Journal of Physics: Conference Series

PAPER • **OPEN ACCESS**

Annual modulation search by XMASS-I with 2.7 years of data

To cite this article: Masaki Yamashita and for theXMASS collaboration 2020 *J. Phys.: Conf. Ser.* **1342** 012083

Annual modulation search by XMASS-I with 2.7 years of data

Masaki Yamashita for the XMASS collaboration

Kamioka Observatory, Institute for Cosmic Ray Research, the University of Tokyo, Higashi-Mozumi, Kamioka, Hida, Gifu, 506-1205, Japan
Kavli Institute for the Physics and Mathematics of the Universe (WPI), the University of Tokyo, Kashiwa, Chiba, 277-8582, Japan

E-mail: `yamashita@icrr.u-tokyo.ac.jp`

Abstract. In this work, we conducted annual modulation search for dark matter with 2.7 years of data taking with the XMASS-I detector. A total exposure was 800 live days times 832 kg. When we assume Weakly Interacting Massive Particle (WIMP) dark matter elastically scattering on the xenon target, the exclusion upper limit of the WIMP-nucleon cross section was $1.9\times10^{-41}\mathrm{cm}^2$ at 8 GeV/c^2. For model independent case, without assuming any specific dark matter model, we did not find any modulation signal with a p-value of 0.11 in the 1–20 keV energy region for the null hypothesis.

1. Introduction

The Earth's velocity relative to the dark matter distribution changes as the Earth moves around the Sun and would produce such a modulation at the level of a few % in the dark matter signal rate that should be observable with terrestrial detectors [1]. The DAMA/LIBRA experiment observed annual modulation of its event rate with a 9.3σ significance in 1.33 ton·year of data taken over 14 annual cycles with 100 to 250 kg of NaI(Tl) [2]. Weakly Interacting Massive Particles (WIMPs) are still well motivated among the many candidates for dark matter particles to date. However, the other experiments that report signals interpreted as WIMP dark matter contradict the DAMA/LIBRA result [3]. In this situation, dark matter models with for example electron recoil signal become interesting as they can produce keV energy deposition in the detector as observed by DAMA/LIBRA [4, 5, 6]. Recently, XMASS reported an annual modulation search for dark matter with such aspects [7] and we have taken more than one year cycle of data with more stable detector temperature, pressure, scintillation light yield conditions. Recent annual modulation searches were reported by XENON100 [8], DM-Ice [9] where the detectors were located at Gran Sasso laboratory in Italy and the South Pole, respectively. XMASS tests this modulation hypothesis with the lowest energy threshold of 1keV among those searched in a different environment and underground site.

2. The XMASS experiment

The XMASS-I employs a single phase liquid xenon (LXe) detector to observe only scintillation light without any electric field. The detector is located at Kamioka Observatory with overburden 1,000 m rock (2700 meter water equivalent) in Japan. The detailed design and performance are described in [16]. The detector is immersed in a water Cherenkov detector, 10 m in diameter and 10.5 m in height as an active veto. A vacuum insulated inner copper vessel holds about 1.1 ton of LXe. 642 high quantum efficiency (28-40% at 175 nm) Hamamatsu R10789 PMTs are mounted in an approximate sphere, an average radius of 40 cm, with 832 kg LXe sensitive volume. In addition to the previous annual modulation data set between November 2013 and March 2015, we have taken more data between April 2015 and July 2016. Hereafter, we call the former period as Run 1 and the later period as Run 2. Note that we recovered some small data set in Run 1 and that results about 28.6 days more data compared with the data set of the previous work. The live times of Run 1 and Run 2 are 387.8 and 412.2 days, respectively. The total live time became 800.0 days, thus, the entire exposure was 1.82 ton·day.

3. Calibration

A detailed procedure for calibrations was described in [7]. The scintillation light yield response was traced by irradiating 122 keV γ rays with a ^{57}Co source into the detector every one or two weeks [16, 17]. The absorption and scattering length for the scintillation light as well as the intrinsic light yield of the liquid xenon scintillator are extracted from the ^{57}Co calibration data with the Monte Carlo simulation [16] and their time variation is shown in Fig. 2. It changed gradually from the beginning of the Run 1, however, we had three major changes in the detector condition. (1) the power failure on August 2014, thus, the detector was cooled by the liquid nitrogen through the cooling coil attached to the inner vessel during the outage. (2) Later, the two pulse tube refrigerators for the detector were swapped for maintenance work in December 2014. (3) Finally, by purification work and followed by the gas circulation with a getter in March 2015.

We use two different energy scales in this analysis: 'keV$_{\rm ee}$' represents an electron equivalent energy incorporating all the gamma-ray calibrations in the energy range and 'keV$_{\rm nr}$' denotes the nuclear recoil energy. The energy threshold in this work corresponds to 1.0 keV$_{\rm ee}$ or 4.8 keV$_{\rm nr}$.

4. Data Analysis

Before retrieving time variation information from data, event reduction was performed to reduce background mainly from Cherenkov light from PMT windows and events near the detector wall as standard cuts [7]. Events with 4 or more PMT hits in a 200 ns coincidence timing window without a muon veto were initially selected as an 'ID Trigger'. A 'Timing cut' was applied by rejecting events occurring within 10 ms from the previous event and having a variance in their hit timings of greater than 100 ns. This cut avoid events caused by after-pulses of bright events induced by, for example, high energy γ-rays or alpha particles. A 'Cherenkov cut' removed events which produce light predominantly from Cherenkov emission, in particular from the beta decays of ^{40}K in the PMT photocathode [10]. Finally, we construct likelihood

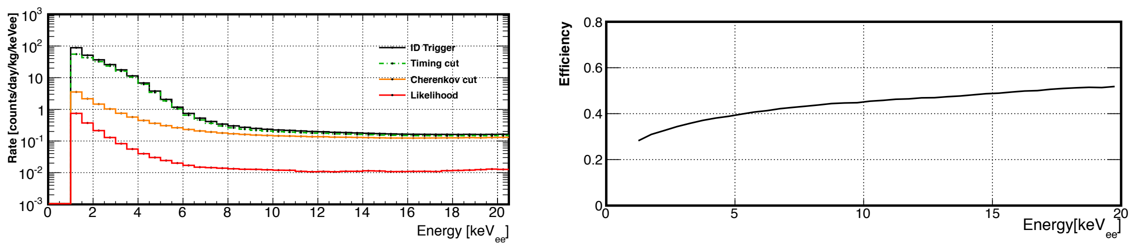

Figure 1. Energy spectrum after each event selection for total exposure (left). Total cut efficiency for uniformly distributed signal events after all cuts (right).

function, $L = f_{sph}(S(\boldsymbol{q})) \times f_{apl}(A(\boldsymbol{q})) \times f_{max}(M(\boldsymbol{q}))$, to remove background events that occurred in front of PMT window or near the detector wall based on PE hits pattern in one event, where $\boldsymbol{q} = (q_1, ..., q_{642})$ is the number of PE for all 642 PMTs in one event. $S(\boldsymbol{q})$, $A(\boldsymbol{q})$, $M(\boldsymbol{q})$ are the parameters based on the $\boldsymbol{q}$ for the sphericity, aplanarity and maximum PE, respectively. f_{sph}, f_{apl} and f_{max} are the probability density functions based on those parameters. The sphericity tensor S^{ij} of an event is defined as $S^{ij} = \sum_{\alpha} q^i_\alpha q^j_\alpha / \sum_{\alpha} q^2_\alpha$, where $i, j = 1, 2, 3$ corresponds to x, y, and z components by taking the detector center as the origin. α is the PMT number, q_α is the observed PE at α-th PMT and $q^{i(j)}_\alpha$ is the PE weighted vector pointing from the detector center to α-th PMT. S^{ij} has three eigenvalues $\lambda_1 \geq \lambda_2 \geq \lambda_3$ $(\lambda_1 + \lambda_2 + \lambda_3 = 1)$ and the sphericity and the aplanarity of the event are defined as $S(\boldsymbol{q}) = \frac{3}{2}(\lambda_2 + \lambda_3)$ and $A(\boldsymbol{q}) = \frac{3}{2}\lambda_3$, respectively. The maximum PE fraction of total PE M is defined as $M(\boldsymbol{q}) = q_{max} / \sum_{\alpha} q_\alpha$. where q_{max} is the maximum PE in one PMT among all PMTs. To optimize the data selection, a log likelihood ratio of signal (uniform) and background near the detector wall, -log(L_s/L_b), was calculated for the final cut. The cut parameter was chosen to keep 50% efficiency after the standard cut by MC. Figure 1 shows the data reduction by those selection and the total cut efficiency after all the cuts, which was evaluated from Monte Carlo simulation with a flat energy spectrum in the sensitive volume.

Systematic errors associated with the PE yield changes during exposure were treated same way as described in [7]. We evaluated the absorption length dependence of the relative cut efficiencies by dividing to 3 energy bins: 1–2 $\mathrm{keV_{ee}}$, 2–6 $\mathrm{keV_{ee}}$ and 6–20 $\mathrm{keV_{ee}}$. We normalize the overall efficiency at an absorption length of 8 m and the relative efficiencies changes from -5% to $+10\%$ for the background events and about -5% to $+4\%$ for the signal events over the relevant absorption range. This is the dominant systematic uncertainty in the present analysis and other systematic errors are negligible [7].

5. Results and Discussion

The data set was divided into 63 time-bins (t_{bins}) with roughly 15 days of real time each. The data in each time-bin were then further divided into energy-bins (E_{bins}) with a width of 0.5 $\mathrm{keV_{ee}}$

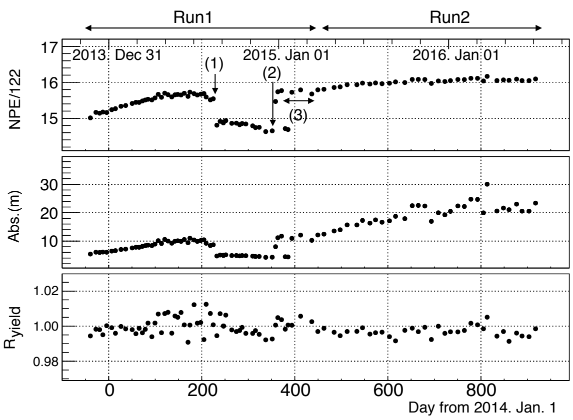

Figure 2. PE yield was monitored by 122 keV γ rays from ^{57}Co (top panel). The absorption length of scintillation light (middle) and relative intrinsic scintillation light yield R_{yield} (bottom) were evaluated by XMASS MC with ^{57}Co calibration data.

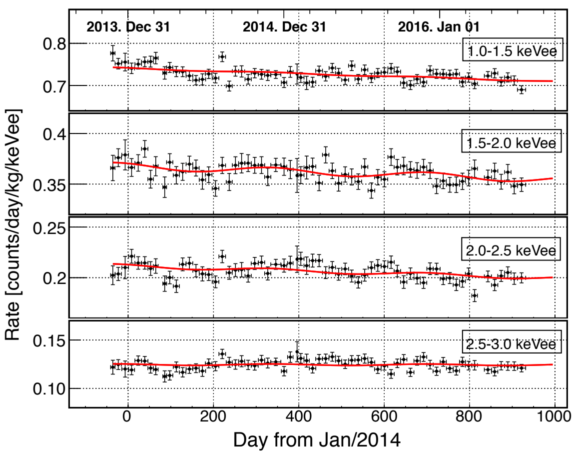

Figure 3. Count rate in 0.5 keV wide bins from 1 to 3 $\mathrm{keV_{ee}}$. The solid curves represent data and best-fit for mode-independent analysis. They have relative, not absolute, efficiency correction.

from 1.0 to 20 keV_{ee}. A pull method was used to fit all energy- and time-bins simultaneously to treat the correlated errors above.

In the case of the WIMP analysis, χ^2 defined as:

$$\chi^2 = \sum_{i}^{E_{bins}} \sum_{j}^{t_{bins}} \left(\frac{(R^{\text{data}}_{i,j} - R^{\text{ex}}_{i,j}(\alpha,\beta))^2}{\sigma(\text{stat})^2_{i,j} + \sigma(\text{sys})^2_{i,j}} \right) + \alpha^2 + \sum^{Nsys} \beta_i^2, \tag{1}$$

where $R^{\text{data}}_{i,j}$, $R^{\text{ex}}_{i,j}$, $\sigma(\text{stat})_{i,j}$ and $\sigma(\text{sys})_{i,j}$ are the data and expected event rate, the statistical and systematic errors of expected event rate for i-th energy and j-th time bin, respectively. A penalty term α represents the size of the relative efficiency error and it is common for all fitted energy bins. Other penalty term, β_i, are parameters for uncertainty of a scintillation efficiency for nuclear recoil [18] and the time constant of nuclear recoil events. The time constant of $26.9\ ^{+0.8}_{-1.2}$ nsec was used based on the neutron calibration with XMASS-I detector. The expected modulation amplitudes become a function of the WIMP mass $A_i(m_\chi)$ as the WIMP mass m_χ determines the recoil energy spectrum. The expected rate in a bin then becomes:

$$R^{\text{ex}}_{i,j}(\alpha,\beta) = \int_{t_j-\frac{1}{2}\Delta t_j}^{t_j+\frac{1}{2}\Delta t_j} \left(\epsilon^b_{i,j}(\alpha) \cdot (B_i t + C^b_i) + \sigma_{\chi n} \cdot \epsilon^s_{i,j} \cdot \left(C^s_i(\beta) + A^s_i(\beta) \cos 2\pi \frac{(t-\phi)}{T} \right) \right) dt, \tag{2}$$

where ϕ and T were the phase and period of the modulation and t_j and Δt_j were the time-bin's center and its width, respectively. $\sigma_{\chi n}$ is the WIMP-nucleon cross section, $\epsilon^b_{i,j}(\alpha)$ and $\epsilon^s_{i,j}(\alpha)$ are the relative efficiency for background and signal, respectively. To account for changing the background rates from long-lived isotopes such as ^{60}Co ($t_{1/2}$ =5.27 yrs) and ^{210}Pb ($t_{1/2}$ =22.3 yrs), we added a simple linear function with B_i for slope and C^b_i for constant in i-th bin. $A^s_i(\beta)$ represents an amplitude and $C^s_i(\beta)$ for unmodulated component for signal in i-th bin. By following Lewin and Smith [15], we assume the most probable speed of v_0=220 km/s, the Earth's velocity relative to the dark matter distribution of $v_E = 232 + 15\ \sin 2\pi(t-\phi)/T$ km/s, and a galactic escape velocity of $v_{esc} = 544$ km/s [19], a local dark matter density of 0.3 GeV/cm^3 for the energy spectrum. To evaluate the sensitivity of WIMP-nucleon cross section, we carried out a statistical test by applying the same analysis to 10,000 dummy samples. The $\pm 1(2)\sigma$ bands in Fig. 4 outline the expected 90% C.L. upper limit band. As we found no significant signal, the 90% C.L. upper limit on the WIMP-nucleon cross section was set for each masses as shown in Fig. 4. The exclusion upper limit of 1.9×10^{-41}cm^2 at 8 GeV/c^2 was obtained.

For the model independent analysis, the expected event rate was estimated as:

$$R^{\text{ex}}_{i,j} = \int_{t_j-\frac{1}{2}\Delta t_j}^{t_j+\frac{1}{2}\Delta t_j} \left(\epsilon^s_{i,j} A^s_i \cos 2\pi \frac{(t-\phi)}{T} + \epsilon^b_{i,j}(\alpha)(B_i t + C^b_i) \right) dt, \tag{3}$$

where the free parameters C^b_i and A^s_i were the unmodulated event rate and the modulation amplitude, respectively. T and ϕ were fixed to 365.24 days and 152.5 days, respectively. The observed count rate after cuts as a function of time in the energy region between 1.0 and 3.0 keV_{ee} is shown in Fig. 3. For an easy-visualization, the data points were corrected by the relative efficiency based on the best fit parameter. For the best fit parameters for a modulation and null hypothesis, $\chi^2_1/\text{ndf} = 2308/2279$ and $\chi^2_0/\text{ndf} = 2357/2317$ were obtained, respectively. The positive (negative) upper limit was obtained as $0.96\ (-1.5) \times 10^{-2}$ events/day/kg/keV_{ee} between 1.0 and 1.5 keV_{ee} and the limits become stricter at higher energy. As a guideline, we make direct comparisons with other experiments not by considering a specific dark matter model but amplitude count rate. The modulation amplitude of $\sim 2 \times 10^{-2}$ events/day/kg/keV_{ee} between 2.0 and 3.5 keV_{ee} was obtained by DAMA/LIBRA [2] and XENON100 reported $1.67\pm0.73\times10^{-3}$ events/day/kg/keV_{ee} (2.0–5.8 keV_{ee}) [8]. This study obtained 90% C.L positive upper limits of $(1.3-3.2)\times10^{-3}$ events/day/kg/keV_{ee} and gives the more stringent constraint.

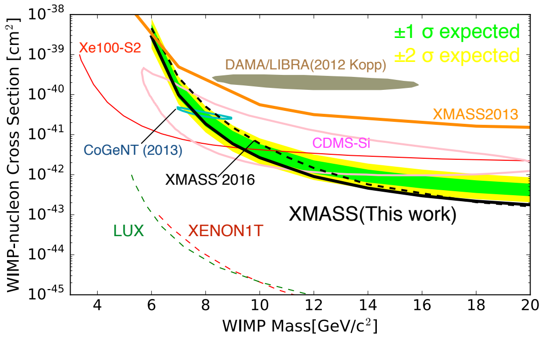

Figure 4. Limits on the spin-independent WIMP-nucleon cross section. The solid black line shows the XMASS 90% C.L. exclusion with other expermenst [3, 10, 12, 11, 13, 14].

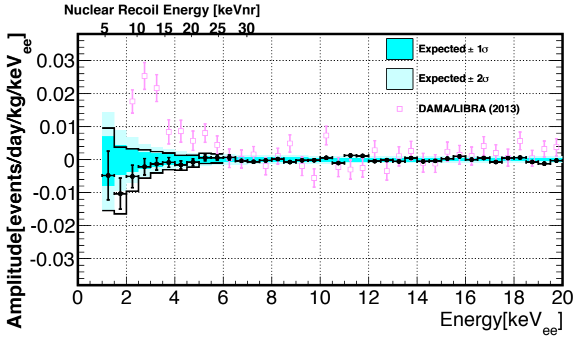

Figure 5. Modulation amplitude for the model independent analyses together with DAMA/LIBRA [2]. Solid lines represent 90% positive (negative) upper limits on the amplitudes.

6. Conclusions

In conclusion, XMASS-I conducted an annual modulation search with 2.7 years data. For the WIMP analysis, the exclusion 90% C.L. upper limit of 1.9×10^{-41}cm^2 at 8 GeV/c^2 was obtained and the result excludes the DAMA/LIBRA allowed region. As for the model independent case, the analysis was carried out from the energy threshold of 1.0 keV$_{ee}$ which is lower than DAMA/LIBRA and XENON100. We did not find any modulation signal and we gave the positive (negative) upper limit amplitude of 0.96 $(-1.5) \times 10^{-2}$ events/day/kg/keV$_{ee}$ between 1.0 and 1.5 keV$_{ee}$ and $(1.3-3.2)\times10^{-3}$ counts/day/kg/keV$_{ee}$ between 2 and 6 keV$_{ee}$. As this analysis does not consider only nuclear recoils, a simple electron or gamma ray interpretation of the DAMA/LIBRA signal can also obey this limit.

References

[1] A. K. Drukier, K. Freese and D. N. Spergel, Phys. Rev. D **33** (1986) 3495.
[2] R. Bernabei et al., Eur. Phys. J. C (2013) 73:2648.
[3] J. Kopp *et al.* JCAP **03** (2012) 001.
[4] J. Kopp et al, Phys. Rev. D **80** (2009) 083502.
[5] B. Feldstein, P. W. Graham, S Rajendran, Phys. Rev. D **82** (2010) 075019.
[6] R. Foot, Phys. Rev. D **90** (2014) 121302(R), R. Foot, arXiv:1508.07402 (2015).
[7] K. Abe *et al.* (XMASS collaboration), Phys. Lett. B **759** (2016) 272.
[8] E. Aprile *et al.* (XENON100 collaboration) Phys. Rev. Lett. **118** (2017) 101101.
[9] E. Barbosa de Souza *et al.* (DM-Ice collaboration), Phys. Rev. D **95** (2017) 032006. of the event
[10] K. Abe *et al.* (XMASS collaboration), Phys. Lett. B **719** (2013) 78.
[11] E. Aprile *et al.* (XENON collaboration), arXiv:1705.06655v2.
[12] D.S. Akerib *et al.* (LUX collaboration), Phys. Rev. Lett. **118** (2017) 021303.
[13] C. E. Aalseth *et al.* (CoGeNT collaboration), Phys. Rev. D **88** (2013) 012002.
[14] R. Agnese *et al.* (CDMS collaboration), Phys. Rev. Lett. **111** (2013) 251301.
[15] J.D. Lewin and P.F. Smith, Astroparticle Phys. **6** (1996) 87.
[16] K. Abe *et al.* (XMASS collaboration), Nucl. Instr. Meth. A **716** (2013) 78.
[17] N. Y. Kim *et al.* , Nucl. Instr. Meth. A **784** (2015) 499.
[18] E. Aprile *et al.*, Phys. Rev. Lett. **107** (2011) 131302.
[19] M.C. Smith *et al.*, Mon. Not. R. Astron. Soc. **379** (2007) 755-772.